Emerging Trends in Biomaterials Research

Understanding the Role of ECM Protein Composition and Geometric Micropatterning for Engineering Human Skeletal Muscle

Rebecca M. Duffy,[1] Yan Sun,[1,2] and Adam W. Feinberg[1,3]

[1]Regenerative Biomaterials and Therapeutics Group, Department of Biomedical Engineering, Carnegie Mellon University, 700 Technology Dr., Pittsburgh, PA 15219, USA; [2]Key Laboratory for Biomechanics and Mechanobiology of Ministry of Education, School of Biological Science and Medical Engineering, Beihang University, Beijing, China; and [3]Department of Materials Science and Engineering, Carnegie Mellon University, Pittsburgh, PA 15219, USA

Associate Editor Akhilesh K Gaharwar oversaw the review of this article.

Abstract—Skeletal muscle lost through trauma or disease has proven difficult to regenerate due to the challenge of differentiating human myoblasts into aligned, contractile tissue. To address this, we investigated microenvironmental cues that drive myoblast differentiation into aligned myotubes for potential applications in skeletal muscle repair, organ-on-chip disease models and actuators for soft robotics. We used a 2D *in vitro* system to systematically evaluate the role of extracellular matrix (ECM) protein composition and geometric patterning for controlling the formation of highly aligned myotubes. Specifically, we analyzed myotubes differentiated from murine C2C12 cells and human skeletal muscle derived cells (SkMDCs) on micropatterned lines of laminin compared to fibronectin, collagen type I, and collagen type IV. Results showed that laminin supported significantly greater myotube formation from both cells types, resulting in greater than twofold increase in myotube area on these surfaces compared to the other ECM proteins. Species specific differences revealed that human SkMDCs uniaxially aligned over a wide range of micropatterned line dimensions, while C2C12s required specific line widths and spacings to do the same. Future work will incorporate these results to engineer aligned human skeletal muscle tissue in 2D for *in vitro* applications in disease modeling, drug discovery and toxicity screening.

Keywords—Skeletal muscle, Tissue engineering, Extracellular matrix, Microcontact printing.

ABBREVIATIONS

ECM	Extracellular matrix
LAM	Laminin
FN	Fibronectin
Col I	Collagen I
Col IV	Collagen IV
SkMDCs	Skeletal muscle derived cells
μCP	Microcontact printed
MFI	Myotube fusion index (nuclei/myotube)
PDMS	Polydimethylsiloxane

INTRODUCTION

Skeletal muscle is composed of billions of molecular motors that are organized into a contractile, multiscale system that provides force generation for a diverse array of living organisms.[36] During the process of myogenesis, myoblasts align with one another, fuse membranes to form myotubes, and then begin to assemble the internal cell machinery into organized sarcomeres of myosin heavy chain (MHC) and actin, the portions of skeletal muscle that serve as actuators at the sub-cellular level.[7,41] Skeletal muscle has unique capabilities including the ability to repair minor injuries and adapt to workloads by increasing volumetric muscle mass. However, in humans this ability to maintain or restore normal structure and function becomes impaired during disease and injury. Understanding how these repair and regeneration mechanisms work is therefore critical to developing new regenerative therapies for skeletal muscle diseases as

Address correspondence to Adam W. Feinberg, Regenerative Biomaterials and Therapeutics Group, Department of Biomedical Engineering, Carnegie Mellon University, 700 Technology Dr., Pittsburgh, PA 15219, USA. Electronic mail: feinberg@andrew.cmu.edu

well as for applications in *in vitro* pharmaceutical testing and as actuators for soft robotics and bioprosthetics.[10] Here we were specifically interested in understanding the role the extracellular matrix (ECM) plays in driving functional skeletal muscle formation since the ECM provides specific architectural and biochemical cues that guide tissue formation *in vivo*. Researchers have demonstrated that the cell-ECM interface can be leveraged to engineer skeletal muscle in 2D and 3D *in vitro* systems,[23,27] and ECM from decellularized tissues has been used to promote regeneration of skeletal muscle defects in human patients.[31]

Engineering skeletal muscle tissue *in vitro* requires an understanding of the microenvironmental cues that drive myogenesis, including ECM composition and architecture, as well as species specific differences as we transition to human systems. A number of *in vitro* studies have shown that myotube formation and contractility depends on specific microenvironmental cues including stiffness,[13,14,35] patterning of ECM proteins,[3,18,46] and ECM composition.[27] However, a quantitative understanding of how specific ECM proteins and their spatial patterning controls skeletal muscle differentiation and alignment is still needed. Skeletal muscle has been engineered from a variety of species *in vitro*, but it has proved much more difficult to differentiate and maintain human skeletal muscle.[12,24] The immortalized C2C12 mouse myoblast cell line is widely studied,[53] and has been used by many researchers to engineer 2D myotube constructs.[19,29,50,57] There are also many examples of 3D engineered skeletal muscle constructs derived from primary rat muscle and fibroblast cocultures,[9] primary chick muscle,[48] primary mouse myoblasts,[49] and C2C12 myoblasts.[40,54] However, there are far fewer examples of engineered human skeletal muscle constructs *in vitro*. Vandenburgh and co-workers established a protocol to engineer contractile human bioartificial muscles that increased in maturity with mechanical stimulation.[37] Recently, Bursac and co-workers developed a method to engineer functional human skeletal muscle constructs that integrated into *in vivo* mouse models and responded to pharmaceutical stimulation.[8,30] However, despite the advances of these 3D engineered human skeletal muscle constructs, they are formed by casting cell within isotropic hydrogels and rely on self-organization to compact into final form. For this reason, 2D platforms are still attractive as tools to better understand the interplay between the ECM and myogenesis in engineered muscle constructs.

The aim of this study was to understand how the composition and microscale geometric patterning of ECM proteins on a surface controls the differentiation of myoblasts into aligned myotubes. Further, we wanted to determine whether the response was species specific and differed between standard murine C2C12s and more clinically relevant human cell lines. Previously, we differentiated C2C12s on micropatterned lines of fibronectin (FN) and quantified how line geometry influenced myotube formation.[46] Specifically, these results led us to investigate how different ECM proteins affected myotube formation and alignment from C2C12 and human primary myoblasts. First, we wanted to determine if ECM proteins found in skeletal muscle would increase myotube differentiation, in terms of density (surface coverage) and length. To test this, we compared myotube differentiation on FN, collagen type IV (Col IV), laminin 111 (LAM), and collagen type I (Col I), which are major components of skeletal muscle ECM.[5,20,32,52] Second, we wanted to determine the critical line width and spacing to uniaxially align myotubes while simultaneously maximizing myotube density and uniaxial alignment. To test this, we differentiated myoblasts on microcontact printed (μCP) ECM protein lines with 10, 15, 20, or 30 μm spacings and 20, 50, 100, or 200 μm widths, as well as on isotropically coated controls. Finally, we wanted to determine whether cell source affected myoblast response to ECM guidance cues. To test this, we differentiated C2C12 mouse myoblasts and human skeletal muscle derived cells (SkMDCs) on these ECM line patterns.

MATERIALS AND METHODS

Substrate Fabrication

The ECM protein micropatterned substrates were fabricated based on previously published techniques.[22,46] Briefly, Sylgard 184 polydimethylsiloxane (PDMS; Dow Corning Corp.) base and curing agent were mixed at a 10:1 mass ratio, respectively. PDMS was spincoated onto 25 mm diameter glass coverslips at 4000 rpm to create an approximately 15 μm thick PDMS layer. PDMS coated coverslips were cured at 65 °C for at least 4 h before use. PDMS stamps for μCP were fabricated as previously described with the exception that MF-26A (Dow Electronic Materials) was used as the developer for the SPR 220.3 positive photoresist (MicroChem Corp.).[46] PDMS stamps with 10, 15, 20, and 30 μm line spacings and 20, 50, 100, and 200 μm line widths were created for a total of 16 micropattern conditions. Patterns are referred to as width × spacing (e.g., a pattern with 50 μm lines and 10 μm spacings is 50 × 10).

All ECM proteins used for μCP were diluted with distilled water to final concentrations of 50 μg/mL for human FN (Sigma-Aldrich), 200 μg/mL for mouse

LAM (Life Technologies), 200 μg/mL for mouse Col IV (Life Technologies), and 500 μg/mL for rat tail Col I (Corning). The procedure for μCP was followed as previously described.[46] Briefly, PDMS stamps were sonicated feature side up for 30 min in 50% ethanol solution. Stamps were dried with a nitrogen air gun, the feature side was coated with protein solution and incubated for 1 h at room temperature. Stamps were rinsed twice in distilled water and dried with the nitrogen gun. PDMS coated coverslips were UV ozone treated for 15 min and stamps were inverted and placed in conformal contact with the coverslip for 5 min to transfer the ECM protein lines. Stamps were then removed, and the patterned coverslips were incubated with 1% w/v Pluronic F-127 solution for 5 min followed by three rinses of phosphate buffered saline (PBS). For isotropically coated coverslips, UV-ozone treated PDMS coverslips were inverted onto 200 μL of protein solution for 15 min, followed by three rinses of PBS. Samples were used immediately or stored in PBS at 4 °C for up to 2 weeks.

Cell Culture

Reagents were obtained from Life Technologies unless indicated otherwise. The murine C2C12 cell line (CRL-1722, ATCC) was cultured and differentiated as recommended by the supplier at 37 °C and 10% CO_2. Cells were cultured and expanded in growth media (GM) [high glucose DMEM (Corning) supplemented with 10% fetal bovine serum, 1% penicillin–streptomycin, and 1% L-glutamine (200 mM)] and split at 1:10 ratios at 80% confluence. Cells were used at < 12 passages from the supplier and were seeded at a density of 30,000 cells/cm^2 on micropatterned substrates. C2C12s proliferated in growth media on substrates for 24–48 h in order to reach 100% confluence on micropatterned lines. Growth media was then exchanged for differentiation media (DM) (high glucose DMEM (Corning) supplemented with 2% horse serum, 1% penicillin–streptomycin, and 1% L-glutamine (200 mM)), and exchanged daily for 6 days. After differentiation, samples were ready to be fixed and stained for analysis of myotube formation as described below.

Human SkMDCs were obtained from Cook MyoSite. Cells were cultured according to the supplier recommendations at 37 °C and 5% CO_2. Additionally, cells were maintained below 80% confluence in MyoTonic Growth Medium (Cook Myosite) during expansion. Cook's SkMDCs were seeded on substrates at 40,000 cells/cm^2 and were switched to MyoTonic Differentiation Medium (MDM—Cook Myosite) after cells reached confluence on patterned lines. MDM was exchanged every 48 h for 6 days. After differentiation, samples were fixed and stained for analysis of myotube formation.

Immunofluorescence Staining and Imaging

Samples were fixed, stained for myotubes, and imaged to quantify myotube formation as previously described.[46] Reagents were obtained from Life Technologies unless otherwise indicated. After 6 days in DM, myotubes were rinsed in PBS (0.625 mM Mg^{2+} and 0.109 mM Ca^{2+}) and fixed with 0 °C methanol (Fisher Scientific) for 2 min. Samples were then rinsed with PBS 3 times for 5 min and incubated with 5% v/v goat serum in PBS for 1 h. Samples were rinsed in PBS 3 times for 5 min prior to incubating for 1 h with 1:200 and 1:100 dilutions of DAPI and monoclonal mouse MHC antibody in PBS, respectively. Samples were rinsed three times with PBS and incubated for 1 h with a 1:100 dilution of Alexa Fluor 555 conjugated with goat anti-mouse antibody. Samples were again rinsed three times in PBS prior to being mounted onto slides using Prolong Gold Anti-fade. Samples were imaged using a Zeiss LSM 700 laser scanning confocal microscope to obtain z-stacks and tile scans of samples. Tile scans were typically 1.28 mm × 1.28 mm. Some tile scans for myotube length were between 2.56 mm × 0.64 mm and 4.48 mm × 0.64 mm in order to ensure that a measurable number of myotubes did not extend out of the field of view for length and myotube fusion index (MFI) measurements.

Image Analysis

Post-processing of images was performed as previously described.[42,46] MHC staining was used to identify myotubes and DAPI to identify nuclei. Percent area myotubes, MFI—or nuclei/myotube, and myotube length were used as metrics for myotube maturity. We also measured myotube alignment relative to the μCP ECM lines. ImageJ was used to quantify all of these metrics using images with immunofluorescent MHC staining. To quantify percent area myotubes, the MHC channel was isolated, thresholded, converted to an 8-bit binary, and holes where nuclei had been were filled using the 'fill holes' feature within the binary menu. The percent of MHC positive pixels were then quantified using the 'analyze particles' feature. Myotube lengths and orientation were measured manually using the line tool, and MFI was quantified manually using the cell counter plug-in. Myotubes that extended outside of the field of view were not quantified for length, MFI, or orientation.

Statistical Analysis

All statistics were performed using SigmaPlot (Systat Software Inc.). Statistical analyses were performed as one-way ANOVA or ANOVA on ranks as deemed appropriate based on normality and equal variance

tests. Data that failed normality or equal variance tests are reported as median (med) and interquartile range; data that passed normality and equal variance tests are presented as mean $\pm$ SD. The following post hoc tests were used: Student–Newman–Keuls Method (Fig. 2d), Dunn's method (Figs. 2e, 2f, 4b, 4c, 4d, 5e, 5f, and 5g), and Holm–Sidak Method (Figs. 4a and 7a, Supplemental Figs. 4 and 5). Differences were considered statistically significant at $p < 0.05$.

RESULTS

C2C12 Differentiation Into Myotubes is Dependent on ECM Composition and Patterning

To investigate how specific ECM proteins influenced the differentiation of myoblasts into myotubes we compared C2C12 myotube formation on FN, LAM, Col IV, and Col I. First, we screened myotube formation on cover slips micropatterned with 100×20 lines or uniformly coated with the ECM proteins as isotropic controls (Fig. 1). The 100×20 lines were selected based on our previous studies that showed FN lines with these dimensions guided formation of aligned myotubes from C2C12 cells.[46] Qualitative results showed that all surfaces supported myoblast adhesion and spreading at day 0 in GM, however by day 6 in DM, cells were no longer attached to the cover slip (delaminated) on isotropic Col I and micropatterned lines of Col I and Col IV. The delamination from the micropatterned lines of Col I and IV began after the switch to DM (see Supplemental Figs. 1 and 2). This demonstrated adhesion of myoblasts during differentiation depended on both the ECM protein composition and patterning in 2D.

To understand this further, we next differentiated C2C12s into myotubes, as measured by MHC positive cells, and quantified myotube length, MFI, and myotube area on micropatterned lines of FN, Col IV, and LAM. Note that we included Col IV in the analysis for comparison; even though most of the cells had delaminated once switched to DM, and by day 6 in DM there were very few myotubes present (Supplemental Fig. 2). Results showed that differentiation was highly dependent on ECM protein composition (Fig. 2a–2c). The C2C12s on the micropatterned LAM lines differentiated into a significantly greater number of myotubes based on MHC positive cells (Fig. 2d), were significantly longer (Fig. 2e), and had significantly higher MFI (Fig. 2f) than cells on FN or Col IV. Importantly, the LAM surface outperformed the FN surface, which we previously showed was effective for engineering anisotropic 2D skeletal muscle tissue and which other groups have used to pattern cardiac

muscle[15,16] and vascular smooth muscle.[1,2] The median values for myotube area and MFI on LAM were 1.5- and 2-times those on FN, respectively. This indicates that LAM increased the total number of myoblasts that differentiated into myotubes as well as the number of myoblasts that fused into a single myotube.

LAM Line Width and Spacing Dictates C2C12 Myotube Differentiation and Alignment

Based on the results of the ECM screen (Fig. 2), we next investigated LAM micropatterned line width and spacing to determine how geometric cues influenced myotube differentiation and uniaxial alignment. We evaluated 16 conditions consisting of 20, 50, 100, and 200 μm line widths and 10, 15, 20, and 30 μm line spacing in addition to an isotropic control (Fig. 3, Supplemental Fig. 3a). These conditions were chosen based on previous results using micropatterned FN lines in our own studies and in the literature.[46,56] As expected, the isotropic control sample had C2C12 myotubes oriented in all directions, as confirmed by the MHC stain and histogram of myotube alignment angle (Supplemental Fig. 3a and 3b). At the 10 μm line spacing, the myotubes were able to bridge between the micropatterned lines and as a result aligned at a 20° to 30° angle to the lines (Fig. 3). At the wider 15, 20, and 30 μm line spacing the myotubes generally followed the micropatterned lines, though there were clear differences in myotube differentiation, orientation, length and MFI.

Next, we quantified the myotube formation on the micropatterned LAM lines in order to determine the patterns that maximized the amount of uniaxially aligned muscle tissue. Similar to our previous results on FN lines,[45] the width and spacing of micropatterned LAM lines had a significant impact on myotube differentiation (Fig. 4a). Myotube area was comparable to the isotropic controls at the 10 and 15 μm line spacing for all line widths. However, the myotubes on these surfaces bridged between the LAM lines at these narrower spacings. The width of the LAM lines was also found to be an important factor, especially at the 20 and 30 μm line spacing. Differentiation was clearly lowest for the 20 μm line width and increased to a maximum level for the 200 μm line width. However, this seemed to be due to differences in LAM surface area, as normalizing the myotube area by the LAM surface area showed statistically equivalent results for all line widths (Supplemental Fig. 4). Myotube orientation generally showed a trend that was opposite to that of myotube area, with uniaxial alignment being better for surface patterns that had lower myotube area. Myotubes grown on lines with spacings of 10 and 15 μm grew aligned relative to each other (Fig. 4b), but these spacings enabled bridging across the spacings, resulting in myo-

Isotropic

100 μm lines

Day 0	Day 6	Day 0	Day 6
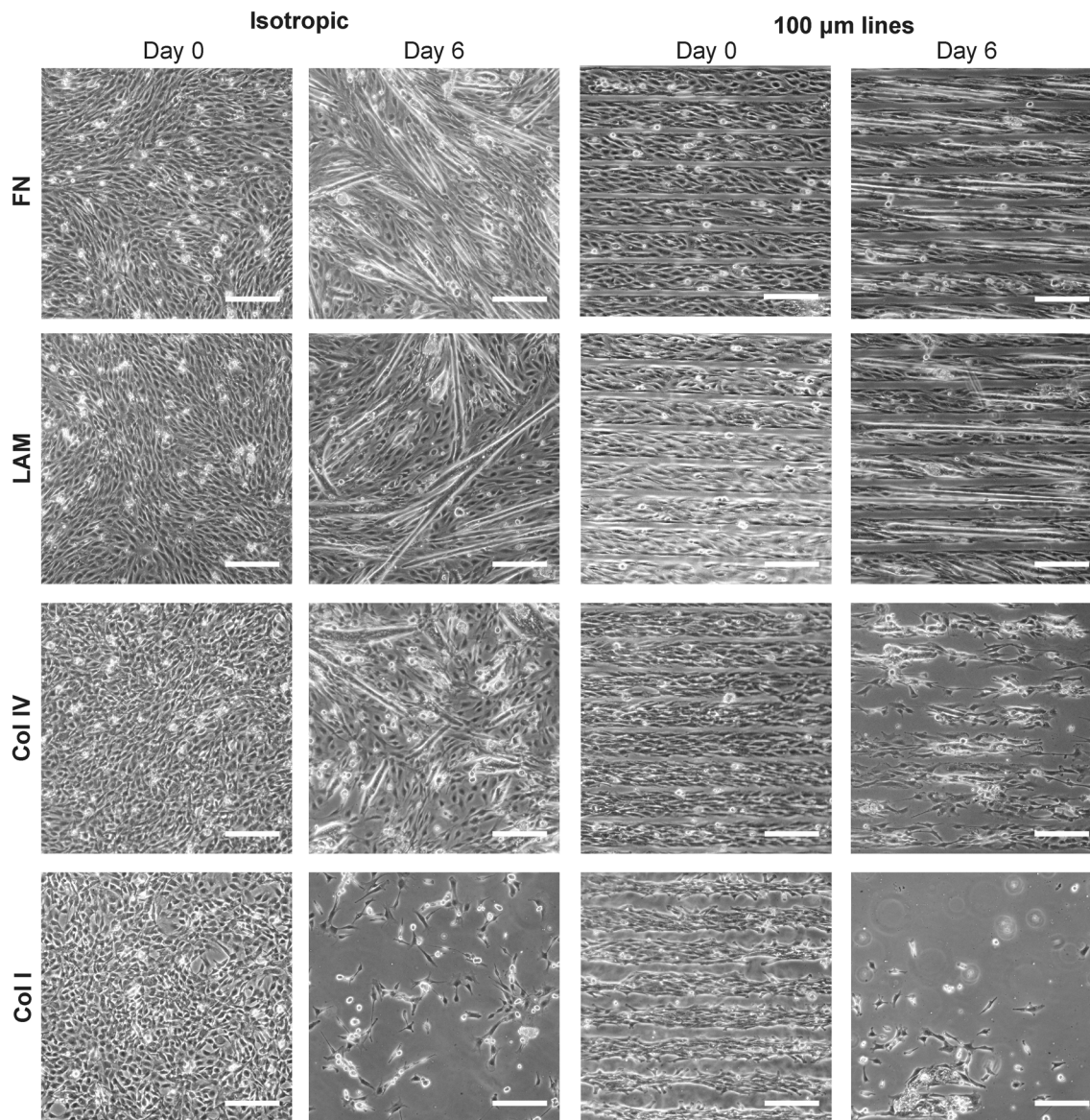
FIGURE 1. Phase contrast images of C2C12 cells differentiated on FN, LAM, Col IV, and Col I. Samples were differentiated on isotropically coated coverslips and 100 × 20 micropatterns. After 6 days of differentiation, cells begin to delaminate from μCP lines of Col IV and Col I and isotropically coated Col I. However, myotubes were able to form on both μCP or isotropically coated LAM and FN. Scale bars 200 μm.

tubes oriented off axis to the micropatterned lines. The 20 and 30 μm line spacings resulted in uniaxial myotube alignment and prevented myotubes from bridging across LAM lines (Fig. 4b). However, on the wider LAM lines, particularly 100 and 200 μm wide lines, the myotubes also began to orient off axis to the pattern. Finally, myotube length (Fig. 4c) and MFI (Fig. 4d) were similar across most of the micropatterns, with the exception that both metrics were significantly lower on the 20 × 20 and 20 × 30 patterns compared to the wider line widths. Note that myotube length and MFI were not calculated for the 10 μm spacing because the myotubes did not align well with the pattern and thus

were not considered effective for engineering aligned skeletal muscle. Thus, the micropatterns that had the best uniaxial alignment parallel to the lines were also the patterns with the lowest myotube area. Additionally, myotubes differentiated on the 100 and 200 μm wide lines had trends towards longer myotubes length and higher MFI compared to isotropic controls, which suggested that that this more organized guidance of myotube fusion resulted in more mature myotubes. In total, these results suggested that LAM line geometry influenced C2C12 myotube formation and that patterns that increased differentiation decreased uniaxial alignment.
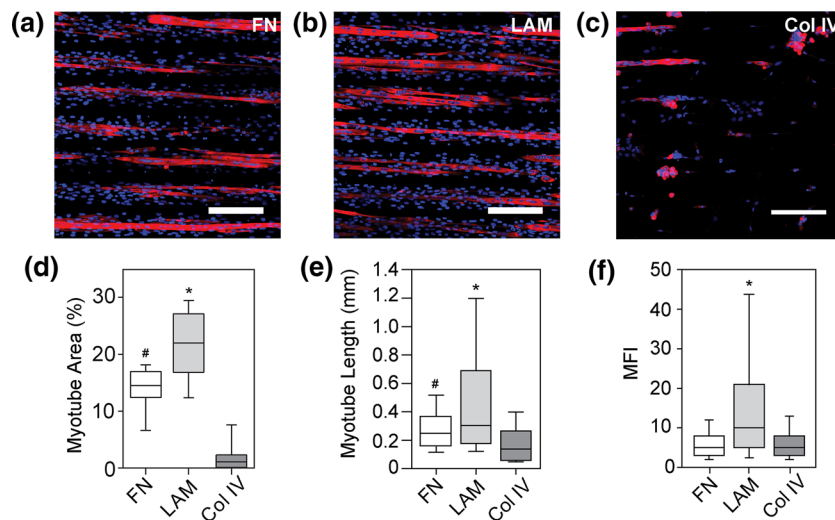
FIGURE 2. C2C12 myotubes differentiated for 6 days on 100 × 20 lines of (a) FN (b) LAM and (c) Col IV show increased myotube formation on LAM and delamination of myotubes from Col IV after staining for MHC and nuclei. (d) Myotubes formed on LAM lines had significantly higher MFI than those differentiated on FN or Col IV. (e) Myotubes differentiated on LAM were significantly longer than those differentiated on FN or Col IV, and myotubes differentiated on FN were also significantly longer than myotubes that formed on Col IV. (f) Percent area of myotubes formed on LAM lines was also significantly higher than on FN or Col IV, and significantly more percent area myotubes formed on FN than on Col IV. *$p < 0.05$ compared to FN and Col I. #$p < 0.05$ compared to Col IV. Scale bars 200 μm. Blue—DAPI; Red—MHC.

Human SkMDCs Differentiation Into Myotubes is Dependent on ECM Composition

To determine if human and mouse myoblasts respond similarly to ECM protein cues, we repeated the ECM protein screen performed for the C2C12 (Fig. 2) for human SkMDCs on Col I, Col IV, FN, and LAM (Fig. 5). The human myotubes differentiated poorly and delaminated on Col I and Col IV (Figs. 5a and 5b), appeared to differentiate marginally better on FN (Fig. 5c) and differentiated robustly on LAM (Fig. 5d). There was significantly greater myotube formation on LAM, greater than 2-times, compared to on Col I, Col IV, and FN (Fig. 5e). Myotubes formed on LAM lines were also significantly more mature as measured by myotube length and MFI. Human myotubes formed on LAM were greater than 3-times longer than myotubes formed on Col I, Col IV, and on FN (Fig. 5f). Similarly, human myotubes formed on LAM had approximately 2-times greater MFI than myotubes formed on Col I and Col IV (Fig. 5g). In total, these results demonstrated that human SkMDCs, which behave as myoblasts in our system, differentiated better on micropatterned LAM lines as compared to the other ECM proteins evaluated.

LAM Line Width and Spacing has Limited Effect on Human SkMDC Myotube Differentiation and Alignment

Next, we performed a smaller pattern screen with human SkMDCs to determine if the different micropatterned LAM line geometries affected human myotube formation similarly to the C2C12 cells. We evaluated nine conditions consisting of 50, 100, and 200 μm wide lines and 10, 15, and 20 μm spacing as well as an isotropic control (Fig. 6, Supplemental Fig. 3c). We did not include 20 μm wide lines as these resulted in poor myotube formation for the C2C12s and did not include 30 μm line spacing because the 20 μm spacing was as effective at aligning myotubes while supporting greater myotube area (Fig. 4). Interestingly, the human myotubes did not behave the same as the C2C12 myotubes and instead became similarly aligned on all LAM micropatterns. All the line patterns had significantly less myotube area than the isotropic control but otherwise were comparable with the 50 × 20 line pattern having approximately half that of myotubes on the 200 × 10, 200 × 15, and 200 × 20 line patterns (Fig. 7a). Normalizing the myotube area by the LAM surface area indicated that the 50 × 20 pattern had significantly less myotube formation, but no statistical differences were observed between the other patterns (Supplemental Fig. 5). Human myotubes on all LAM patterns were uniaxially aligned to the lines, different than the isotropic control (Supplemental Fig. 3D), but with no statistically significant difference between line patterns (Fig. 7b). Myotube orientation only began to deviate from the line pattern at the 200 μm width, as the distribution angles increased (Fig. 7b). Similar to the uniaxial alignment of the human myoblasts on all patterns, there were no statistical significant difference in myotube length
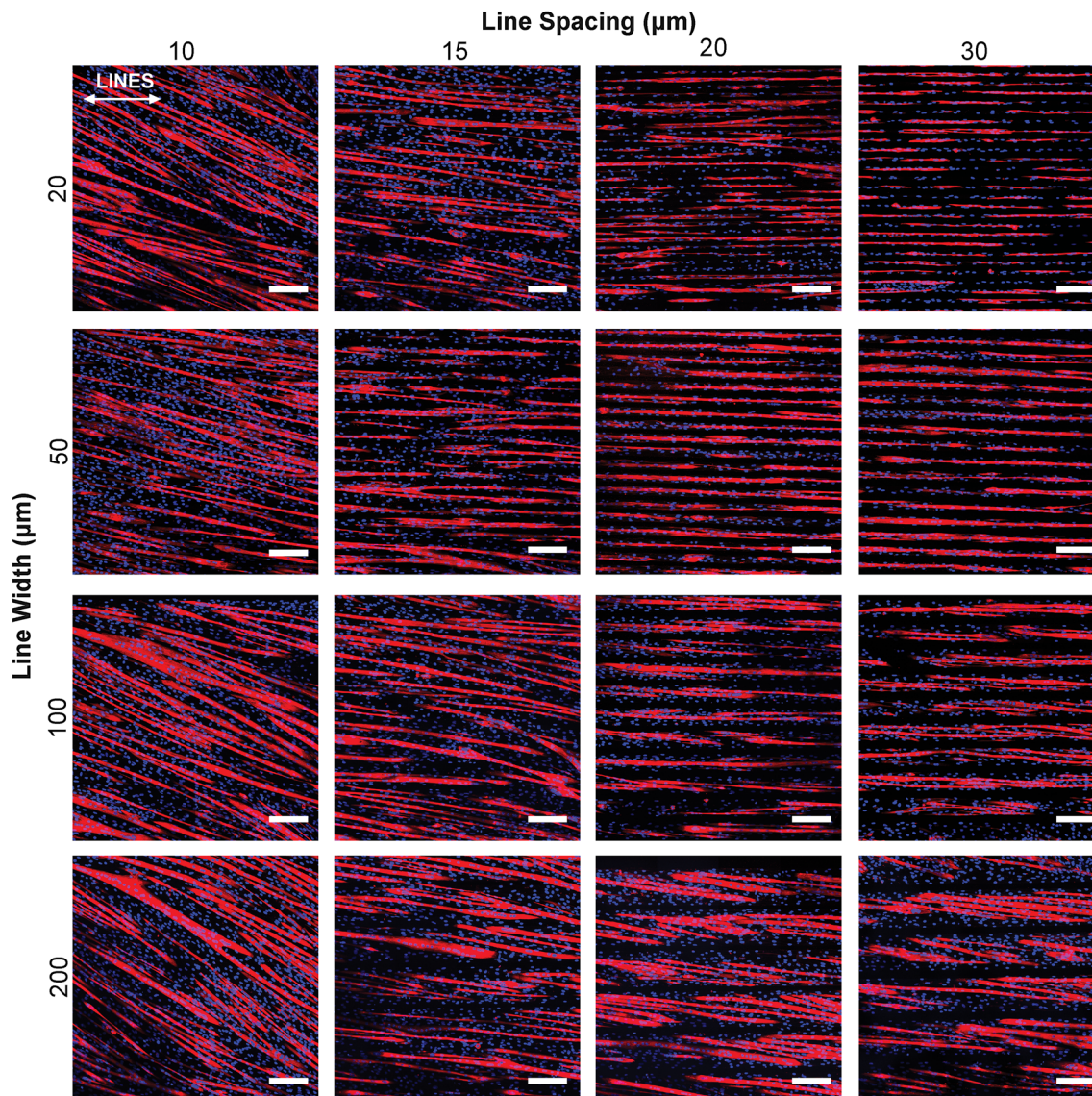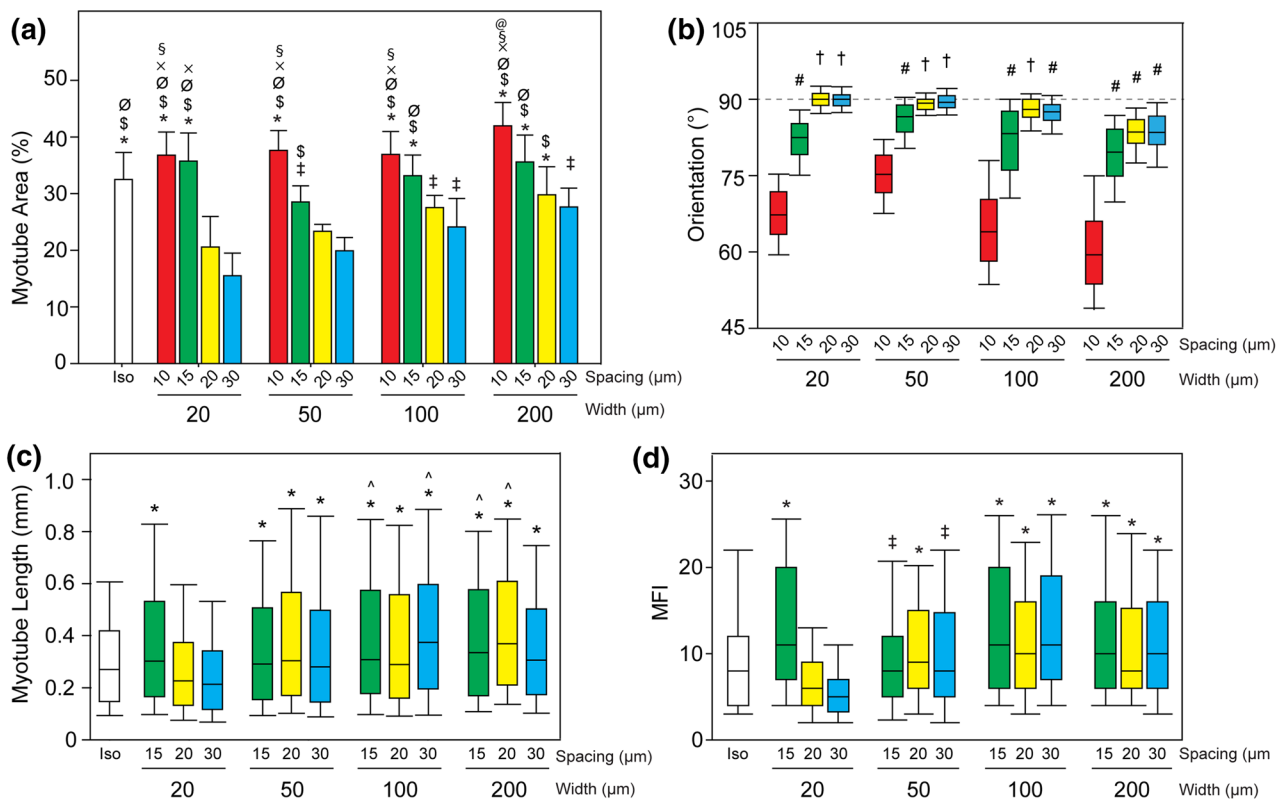
Line Spacing (μm)

FIGURE 3. Representative images of C2C12 cells differentiated on 16 different line patterns of LAM. Myotubes deviate from aligning with the designated pattern when geometric spacing is too narrow (<15 μm), or when the lines are too wide (200 μm). White arrows represent direction of μCP lines. Scale bars 200 μm. Blue—DAPI; Red—MHC.

(Fig. 7c) and MFI (Fig. 7d) between the different LAM line widths and spacings. As a further control to account for lot-to-lot variability, we evaluated five additional human SkMDC lines, and while there were differences in differentiation efficiency, all formed well-aligned myotubes on the LAM patterns. This suggests that our results indicated a difference between species, and were representative of human SkMDC cells.

Micropattern Geometries that Maximize Formation of Aligned Muscle are Species Specific

Finally, we evaluated the data on myotube area and alignment for both C2C12 and human SkMDC cells to directly compare across species. For the C2C12s,

myotube orientation angle was plotted as a function of myotube area, and this confirmed that there was an inverse relationship between these properties (Fig. 8a). While it was possible to achieve myotube areas as high as approximately 40%, it was at the expense of alignment. When taking uniaxial alignment in the direction of the line micropatterns into consideration, the maximum myotube area that could be achieved was much lower at approximately 25%. In contrast, for the human SkMDCs, the relationship between myotube orientation angle and myotube area was completely different, showing minimal dependence on the micropattern geometry (Fig. 8b). For all conditions the human myotubes were uniaxially aligned in the direction of the micropatterned lines. The human

FIGURE 4. (a) Percent area myotubes is higher on 10 and 15 μm spacing conditions because myotubes have more patterned area of LAM on which to form. (b) The orientation of lines is marked at 90°. Myotubes maintain alignment with the patterned ECM when the line spacing is 20 or 30 μm, and line width is <200 μm. (c) Longer myotubes formed on from patterned lines >20 μm wide. (d) Myotubes formed on wider lines were the result of fusion of significantly more myoblasts as measured by MFI. Length and MFI were not quantified for line spacings of 10 μm as myotubes were not restricted to form uniaxially along the pattern. $^{\dagger}p < 0.05$ compared to 10 and 15 μm spacings and all widths; $^{\#}p < 0.05$ compared to 10 μm spacings; $^{*}p < 0.05$ compared to 20 × 20 and 20 × 30; $^{\wedge}p < 0.05$ compared to isotropic; $^{\ddagger}p < 0.05$ than 20 × 30; $^{\$}p < 0.05$ compared to 50 × 30; $^{\varnothing}p < 0.05$ compared to 50 × 20 and 100 × 30; $^{\S}p < 0.05$ compared to 50 × 15 and 200 × 30; $^{\times}p < 0.05$ compared to 100 × 20; $^{@}p < 0.05$ compared to 100 × 15 and 200 × 20.

myotubes we able to bridge across the LAM lines at the narrower line spacings, but this did not cause the myotubes to change their angle of orientation, as it did for the C2C12 myotubes. Thus, increasing myotube area was dependent primarily on the width of the LAM line, and the maximum that could be achieved was approximately 35%. Together, these results highlight the differential response of human and murine skeletal muscle cells to the LAM micropatterned surface, and that even though the C2C12s could achieve a greater myotube area, the human cells achieved a greater uniaxially aligned myotube area.

DISCUSSION

Overall, our results show that myotube formation and uniaxial alignment in 2D engineered skeletal muscle depends on composition and micropatterning of the ECM proteins and the cell source. We observed a tradeoff between myotube orientation and myotube

area for C2C12s that was not observed for human SkMDC derived myotubes. This could be attributed to donor variation in the human cells, but 5 different donor lots differentiated on the same patterns all behaved similarly (Supplemental Fig. 6). Specifically, we observed that line spacings of 10 or 15 μm enabled C2C12 myotubes to bridge between LAM lines and thus did not align to the pattern (Fig. 3). However, these same line spacings were able to align human myotubes on the LAM lines parallel to the pattern (Fig. 5). There are multiple potential reasons for these differences. First, the C2C12s are an immortalized myoblast cell line and behave differently than primary isolated muscle precursor cells. For example, they are more proliferative than human SkMDCs, reaching confluence at a faster rate (data not shown). This rapid C2C12 proliferation rate may lead to transient overcrowding on the lines that facilitated bridging across the smaller 10 and 15 μm line spacings, and subsequent fusing with cells on adjacent lines. In contrast, the human SkMDCs did not proliferate as rapidly and
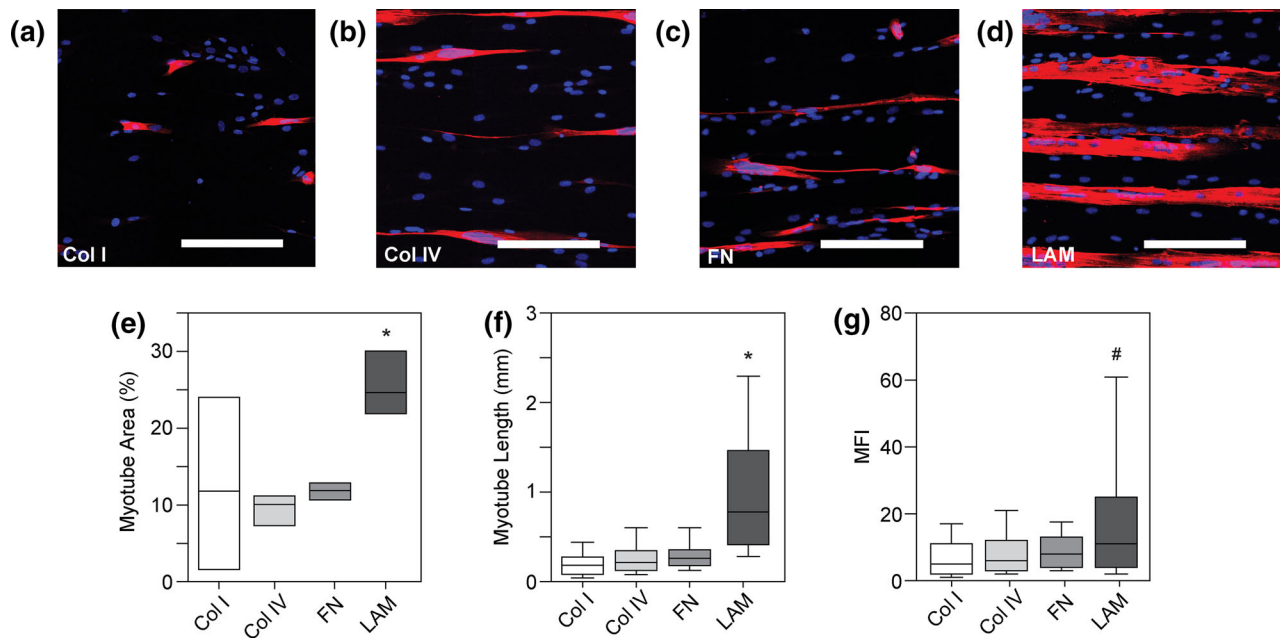
FIGURE 5. (a–d) Representative images of MHC and DAPI staining of human myotube formation on 100 × 20 lines. (e) Quantifying the percent area of myotube formation for human skeletal muscle cells shows significantly higher myotube area on LAM compared to Col I, Col IV, and FN. Myotube formation on Col I is highly variable. (f) Human myotubes formed on LAM lines are significantly longer than myotubes formed on Col I, Col IV, and FN. (g) Human myotubes formed on LAM lines also have significantly higher MFI than those formed on Col I and Col IV lines. *$p < 0.05$ compared to Col I, Col IV, and FN. #$p < 0.05$ compared to Col I and Col IV. Scale bars 200 μm. Blue—DAPI; Red—MHC.

thus fused with cells on the same LAM line. The large size of the myotubes means that they are unlikely to bridge once they have formed. Thus, the difference in response by the murine and human muscle cells may be due in part to intrinsic differences in growth rate. Second, the C2C12s myotubes appeared to have an inherent bias in the direction of alignment relative to the direction of the myotube lines. This was observed on the patterns with 10 and 15 μm spacings as well as on the 100 and 200 μm lines with wider spacings. This was most notable on the 200 × 20 pattern (Figs. 3 and 4b), where the C2C12 myotubes were entirely confined to the 200 μm wide LAM lines but still aligned 5° to 10° off axis to the pattern. We observed the exact same behavior on FN lines in previous work,[45] and other groups have reported similar responses as well for C2C12s on micropatterns.[4,56] Thus, there are clearly genetically encoded similarities and differences in cell response to microenvironmental cues between the C2C12 and human muscle cells.

This raises a number of interesting questions regarding the mechanisms involved in muscle differentiation across species as well as the interplay between physical and biochemical cues in the microenvironment. For example, both murine C2C12 and human SkMDCs demonstrated significantly increased differentiation on LAM lines compared to FN, Col I and Col IV (Figs. 2 and 5). There are multiple potential

reasons for this, but one possibility is the different integrins used to attach to these ECM proteins. As noted, we observed poor differentiation of C2C12s and human SkMDCs on both collagens. This could be related to the fact that a fivefold increase in fibrillary collagens has been observed in very old muscle, as well as increases in $\beta1$ integrin, suggesting that Col I may inhibit myogenesis *in vivo*.[38] Additionally, when porcine myoblasts were differentiated on Col I, gelatin, FN, Matrigel, and LAM, myogenin, a late myogenic marker, was expressed at the lowest levels on Col I.[51] Poor myotube formation has also been observed for murine satellite cells cultured on entactin–laminin–collagen (ECL) substrates, Col IV, poly-D-lysine, and LAM, where higher myotube fusion rates occurred on poly-D-lysine or LAM compared to Col IV or ECL.[6,43] Col IV content in skeletal muscle is also higher in patients with Duchenne muscular dystrophy (DMD) and impaired muscle regeneration,[26] which is consistent with increased Col IV gene expression in DMD myotubes.[55] Similarly, in mouse models of DMD, LAM 111 injections, which increased the relative amount of LAM in the ECM, increased muscle strength in treated mice,[21] and LAM 111 injections in mice with muscle damage induced by eccentric exercise resulted in significantly more embryonic-MHC positive fibers.[58] In addition to integrins, it is also known that dystroglycan (DG) receptor binds to laminin globular
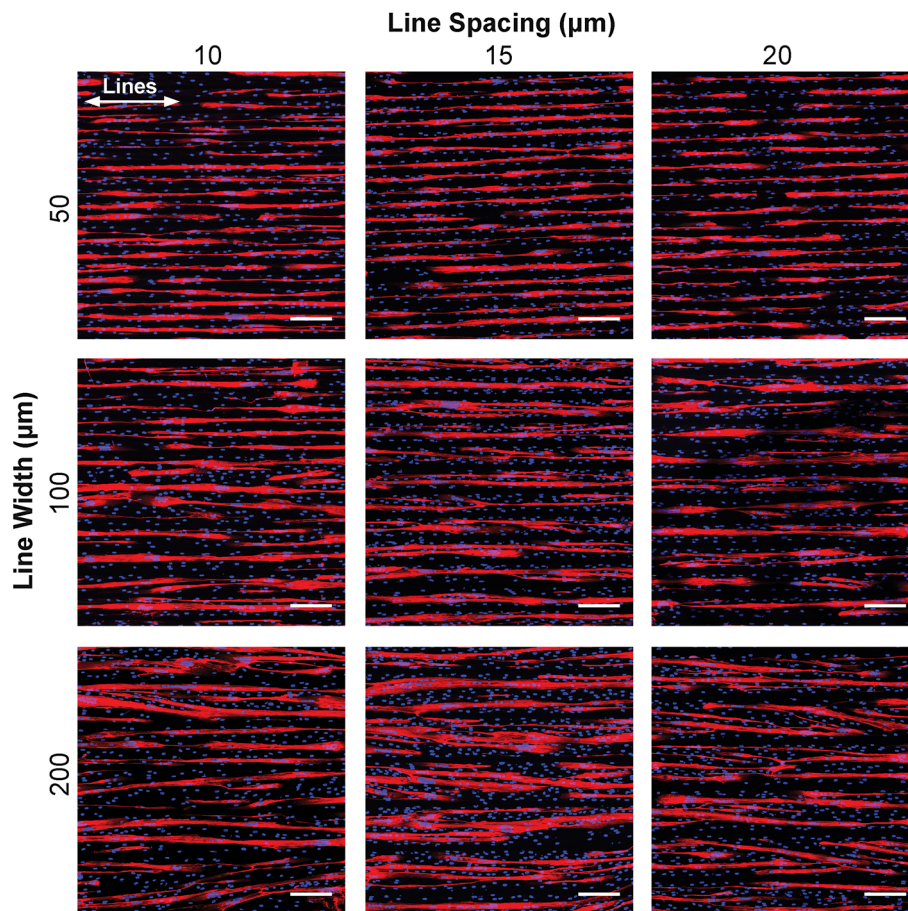
Line Spacing (μm)

FIGURE 6. Representative images of human myotube formation after 6 days of differentiation on 9 line patterns of LAM as well as an isotropic control. Myotubes do not appear to deviate from line patterns with narrow line spacings (<20 μm) to the extent that C2C12 mouse myoblasts do. Scale bars 200 μm. White arrows represent orientation of LAM lines. Blue—DAPI; Red—MHC.

domain 4 on the LAM α1 chain.[11] The DG complex activates pathways that increase myoblast growth[33] and is one of the proteins that is affected by DMD. This results in severe defects in muscle regeneration and eventual loss of structure and function of formerly healthy skeletal muscle.[39,44] In terms of ECM composition, our results and those noted from the literature support the finding that LAM increases murine and human myoblast differentiation into myotubes. However, the reasons for differences in myotube orientation remain unclear and will require further studies to elucidate.

An important aspect of the current study is the delamination of differentiating myotubes on micropatterned lines of Col I and Col IV, which could be influencing the interpretation of our results. Skeletal muscle myotubes are known to form within Col I gels,[40,48,49] so the inability of myotubes to consistently form on micropatterned lines of Col I and Col IV may be an artifact of the μCP method itself. It is possible that the poor myotube differentiation is due to lack of cell and/or ECM adhesion to the underlying PDMS,

contributing to cell and/or myotube delamination during culture. One question is whether the myoblasts detach from the coverslip, or whether the myoblasts fuse into myotubes and then detach. After initial seeding in GM, myoblasts adhered on both micropatterned and isotropically coated coverslips of Col I and Col IV (Fig. 1). However, myoblasts began to detach as early as 24 h after switching to lower serum containing DM, (Supplemental Fig. 1). This would suggest that the loss of cells on the Col I and Col IV occurs prior to fusion into myotubes, perhaps driven by a decrease in fibronectin and vitronectin from FBS removal. It is possible increased cell contractility could result in myoblasts or myotubes detaching from the patterned proteins or peeling the patterned proteins off of coverslips. In fact, even on the FN and LAM micropatterned lines, which support differentiation, myotubes will eventually delaminate after 6–14 days in culture, depending on the specific cell type, ECM protein and micropattern used. Recently it has been shown that covalently crosslinking FN to PDMS using genipin enabled long term smooth
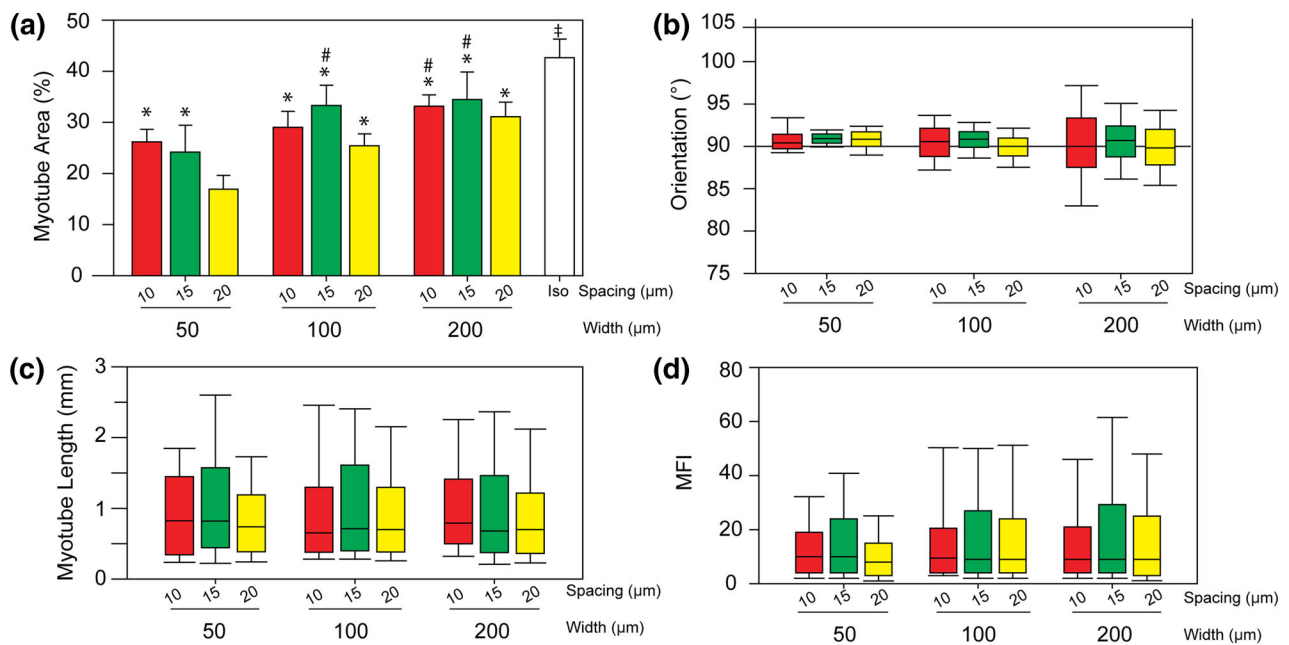
FIGURE 7. (a) Percent area myotubes for each LAM line pattern and isotropic control (not normalized for percent area of patterned LAM) shows an increase in myotube formation as the line width increases, as expected. (b) With 90° representing parallel orientation to the μCP LAM, there was no significant difference in orientation on patterned lines. (c) There is no statistical difference in myotube length or (d) MFI for human myotubes grown on nine different line width and spacing conditions of LAM. *$p < 0.05$ compared to 50 × 20; #$p < 0.05$ compared to 50 × 10, 50 × 15, and 100 × 20; ‡$p < 0.05$ compared to all other conditions.
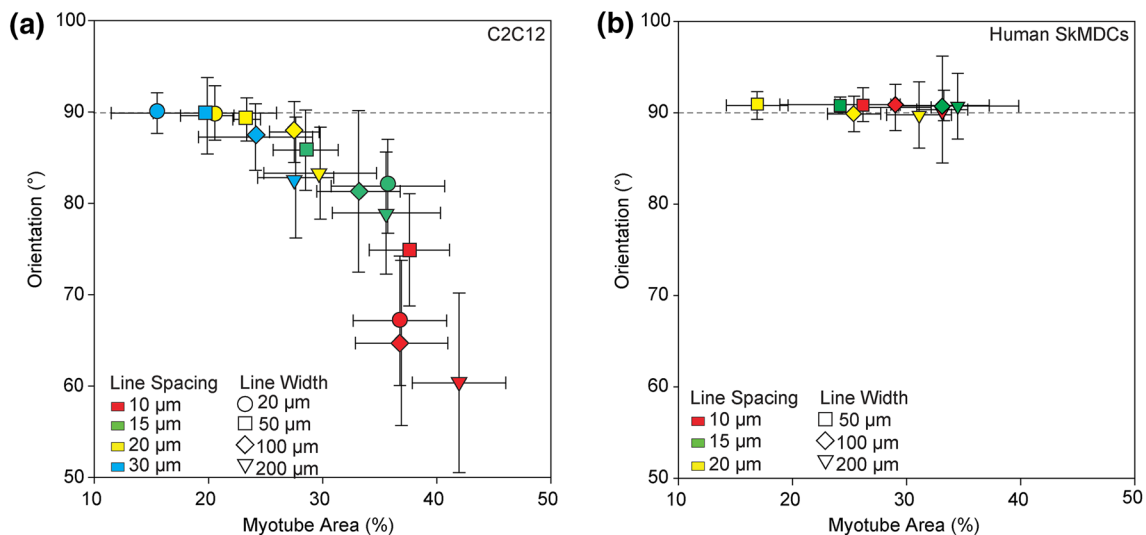
FIGURE 8. (a) Scatterplot of percent area myotubes against the orientation of myotubes for each pattern shows a trend of increasing deviation from alignment with the patterned lines as percent area of myotubes increases. There is a tradeoff for increasing the amount of myotube formation and maintaining uniaxial organization of myotubes. (b) Scatterplot with human myotube orientation and percent area shows there is not a decrease in alignment with LAM lines (90°) with an increase in percent area myotubes and decrease in line spacing, as is observed with C2C12 myotubes. Error bars represent standard deviation.

muscle cell attachment on micropatterned FN lines.[25] This could potentially be applied to future studies with skeletal muscle on patterned lines of Col IV and Col I but was outside the scope of the current study. In general, more in depth studies need to be performed to determine the reason for myoblast or myotube

delamination from these proteins at such an early stage of differentiation. Regardless of the cause, this is an inherent limitation of the 2D micropatterned *in vitro* culture system. However, this 2D approach was used for these studies because it served a starting point that allowed us to probe how ECM composition in con-

junction with micropatterned geometry influenced myotube formation.

Future work will explore the role of ECM composition and micropatterning in more advanced 2D and 3D model systems of engineered skeletal muscle. For 2D systems, we are interested in measuring contractile force generation using our previously developed muscular thin film contractility assay. However, the human myotubes start to delaminate after 6 days but must be matured longer than this to become contractile. It may be possible to solve this problem by crosslinking the LAM to the PDMS using genipin or by increasing the surface area for adhesion by using LAM coated micropatterned ridges. However, we are primarily interested in scaling our current findings to engineered 3D skeletal muscle tissues to allow us to differentiate myotubes for at least 2–4 weeks.[24,27,30,49] An open question is whether LAM can have the same effect in 3D muscle differentiation as in 2D, and if so how LAM must be integrated into the Col I and fibrinogen gels typically used. Further, 3D muscle constructs more readily provide functional metrics of skeletal muscle maturity, such as twitch force and calcium handling dynamics. While it is challenging to precisely micropattern LAM cues in 3D, emerging technologies such as decellularization[28,34] and engineered LAM nanofibers[17,47] suggest that we may be able to engineer 3D scaffolds comparable to our 2D surfaces in the near future.

CONCLUSIONS

In conclusion, we have engineered skeletal muscle from murine C2C12s and human SkMDCs and demonstrated that myotube differentiation and alignment is dependent on ECM protein composition and micropattern geometry. Both C2C12 and human myotube formation was significantly increased on micropatterned LAM, and with poor myotube formation significant delamination on both Col I and Col IV. The C2C12 myotubes required specific geometric cues, line width and spacing, to guide uniaxial myotube alignment compared to human SkMDCs. In general, micropatterns that increased myotube area decreased uniaxial alignment of C2C12 myotubes. In contrast, all LAM line micropatterns guided human SkMDCs to uniaxially align, with no significant differences observed for myotube orientation, length or MFI. This means that myotube formation as guided by ECM composition and geometric cues is species dependent. Looking forward, this means the role of microenvironmental cues is complex, multifactorial and dependent on cell origin. These factors are critical to understand as theses tissue engineering technologies

are translated to clinical applications, and further demonstrates that utility of the 2D platform to screen multiple parameters as lead up to more targeted studies in 3D.

ELECTRONIC SUPPLEMENTARY MATERIAL

ACKNOWLEDGMENTS

REFERENCES

[1]Alford, P. W., A. W. Feinberg, S. P. Sheehy, and K. K. Parker. Biohybrid thin films for measuring contractility in engineered cardiovascular muscle. *Biomaterials* 31:3613–3621, 2010.

[2]Alford, P. W., A. P. Nesmith, J. N. Seywerd, A. Grosberg, and K. K. Parker. Vascular smooth muscle contractility depends on cell shape. *Integr. Biol.* 3:1063–1070, 2011.

[3]Altomare, L., M. Riehle, N. Gadegaard, M. Tanzi, and S. Fare. Microcontact printing of fibronectin on a biodegradable polymeric surface for skeletal muscle cell orientation. *Int. J. Artif. Organs* 33:535–543, 2010.

[4]Bajaj, P., B. Reddy, Jr, L. Millet, C. Wei, P. Zorlutuna, G. Bao, and R. Bashir. Patterning the differentiation of C2C12 skeletal myoblasts. *Integr. Biol. (Camb)* 3:897–909, 2011.

[5]Boonen, K. J. M., and M. J. Post. The muscle stem cell Niche: regulation of satellite cells during regeneration. *Tissue Eng. Part B-Rev.* 14:419–431, 2008.

[6]Boonen, K. J., K. Y. Rosaria-Chak, F. P. Baaijens, D. W. van der Schaft, and M. J. Post. Essential environmental cues from the satellite cell niche: optimizing proliferation and differentiation. *Am. J. Physiol. Cell Physiol.* 296:C1338–1345, 2009.

[7]Charge, S. B., and M. A. Rudnicki. Cellular and molecular regulation of muscle regeneration. *Physiol. Rev.* 84:209–238, 2004.

[8]Cheng, C. S., B. N. Davis, L. Madden, N. Bursac, and G. A. Truskey. Physiology and metabolism of tissue-engineered skeletal muscle. *Exp. Biol. Med. (Maywood)* 239:1203–1214, 2014.

[9]Dennis, R. G., and P. E. Kosnik, 2nd. Excitability and isometric contractile properties of mammalian skeletal muscle constructs engineered *in vitro*. *In Vitro Cell. Dev. Biol. Anim.* 36:327–335, 2000.

[10]Duffy, R. M., and A. W. Feinberg. Engineered skeletal muscle tissue for soft robotics: fabrication strategies, current applications, and future challenges. *Wiley Interdiscip. Rev.-Nanomed. Nanobiotechnol.* 6:178–195, 2014.

[11]Durbeej, M., J. F. Talts, M. D. Henry, P. D. Yurchenco, K. P. Campbell, and P. Ekblom. Dystroglycan binding to laminin alpha1LG4 module influences epithelial morphogenesis of salivary gland and lung *in vitro*. *Differentiation* 69:121–134, 2001.

[12]Eberli, D., S. Soker, A. Atala, and J. J. Yoo. Optimization of human skeletal muscle precursor cell culture and myofiber formation *in vitro*. *Methods* 47:98–103, 2009.

[13]Engler, A. J., M. A. Griffin, S. Sen, C. G. Bonnetnann, H. L. Sweeney, and D. E. Discher. Myotubes differentiate optimally on substrates with tissue-like stiffness: pathological implications for soft or stiff microenvironments. *J. Cell Biol.* 166:877–887, 2004.

[14]Engler, A. J., S. Sen, H. L. Sweeney, and D. E. Discher. Matrix elasticity directs stem cell lineage specification. *Cell* 126:677–689, 2006.

[15]Feinberg, A. W., P. W. Alford, H. Jin, C. M. Ripplinger, A. A. Werdich, S. P. Sheehy, A. Grosberg, and K. K. Parker. Controlling the contractile strength of engineered cardiac muscle by hierarchal tissue architecture. *Biomaterials* 33:5732–5741, 2012.

[16]Feinberg, A. W., A. Feigel, S. S. Shevkoplyas, S. Sheehy, G. M. Whitesides, and K. K. Parker. Muscular thin films for building actuators and powering devices. *Science* 317:1366–1370, 2007.

[17]Feinberg, A. W., and K. K. Parker. Surface-initiated assembly of protein nanofabrics. *Nano Lett.* 10:2184–2191, 2010.

[18]Flaibani, M., L. Boldrin, E. Cimetta, M. Piccoli, P. De Coppi, and N. Elvassore. Muscle differentiation and myotubes alignment is influenced by micropatterned surfaces and exogenous electrical stimulation. *Tissue Eng. Part A* 15:2447–2457, 2009.

[19]Fujita, H., K. Shimizu, and E. Nagamori. Novel method for measuring active tension generation by C2C12 myotube using UV-crosslinked collagen film. *Biotechnol. Bioeng.* 106:482–489, 2010.

[20]Gillies, A. R., and R. L. Lieber. Structure and function of the skeletal muscle extracellular matrix. *Muscle Nerve* 44:318–331, 2011.

[21]Goudenege, S., Y. Lamarre, N. Dumont, J. Rousseau, J. Frenette, D. Skuk, and J. P. Tremblay. Laminin-111: a potential therapeutic agent for duchenne muscular dystrophy. *Mol. Ther.* 18:2155–2163, 2010.

[22]Grosberg, A., P. W. Alford, M. L. McCain, and K. K. Parker. Ensembles of engineered cardiac tissues for physiological and pharmacological study: heart on a chip. *Lab Chip* 11:4165–4173, 2011.

[23]Grounds, M. D., L. Sorokin, and J. White. Strength at the extracellular matrix-muscle interface. *Scand. J. Med. Sci. Sports* 15:381–391, 2005.

[24]Guo, X., K. Greene, N. Akanda, A. Smith, M. Stancescu, S. Lambert, H. Vandenburgh, and J. Hickman. *In vitro* differentiation of functional human skeletal myotubes in a defined system. *Biomater. Sci.* 2:131–138, 2014.

[25]Hald, E. S., K. E. Steucke, J. A. Reeves, Z. Win, and P. W. Alford. Microfluidic genipin deposition technique for extended culture of micropatterned vascular muscular thin films. *J. Vis. Exp.* 100:e52971, 2015.

[26]Hayashi, Y. K., E. Engvall, E. Arikawa-Hirasawa, K. Goto, R. Koga, I. Nonaka, H. Sugita, and K. Arahata. Abnormal localization of laminin subunits in muscular dystrophies. *J. Neurol. Sci.* 119:53–64, 1993.

[27]Hinds, S., W. N. Bian, R. G. Dennis, and N. Bursac. The role of extracellular matrix composition in structure and function of bioengineered skeletal muscle. *Biomaterials* 32:3575–3583, 2011.

[28]Jallerat Q., J. M. Szymanski and A. W. Feinberg. Nano- and Microstructured ECM and Biomimetic Scaffolds for Cardiac Tissue Engineering. In: *Bio-inspired Materials for Biomedical Engineering*. Wiley 2014, pp. 195–226.

[29]Ker, E. D., A. S. Nain, L. E. Weiss, J. Wang, J. Suhan, C. H. Amon, and P. G. Campbell. Bioprinting of growth factors onto aligned sub-micron fibrous scaffolds for simultaneous control of cell differentiation and alignment. *Biomaterials* 32:8097–8107, 2011.

[30]Madden, L., M. Juhas, W. E. Kraus, G. A. Truskey, and N. Bursac. Bioengineered human myobundles mimic clinical responses of skeletal muscle to drugs. *Elife* 4:e04885, 2015.

[31]Mase, Jr., V. J., J. R. Hsu, S. E. Wolf, J. C. Wenke, D. G. Baer, J. Owens, S. F. Badylak, and T. J. Walters. Clinical application of an acellular biologic scaffold for surgical repair of a large, traumatic quadriceps femoris muscle defect. *Orthopedics* 33:511, 2010.

[32]Nakamura, Y. N., H. Iwamoto, T. Yamaguchi, Y. Ono, Y. Nakanishi, S. Tabata, S. Nishimura, and T. Gotoh. Three-dimensional reconstruction of intramuscular collagen networks of bovine muscle: a demonstration by an immuno-histochemical/confocal laser-scanning microscopic method. *Anim. S. J.* 78:445–447, 2007.

[33]Oak, S. A., Y. W. Zhou, and H. W. Jarrett. Skeletal muscle signaling pathway through the dystrophin glycoprotein complex and Rac1. *J. Biol. Chem.* 278:39287–39295, 2003.

[34]Ott, H. C., T. S. Matthiesen, S.-K. Goh, L. D. Black, S. M. Kren, T. I. Netoff, and D. A. Taylor. Perfusion-decellularized matrix: using nature's platform to engineer a bioartificial heart. *Nat. Med.* 14:213–221, 2008.

[35]Palchesko, R. N., L. Zhang, Y. Sun, and A. W. Feinberg. Development of polydimethylsiloxane substrates with tunable elastic modulus to study cell mechanobiology in muscle and nerve. *PLoS One* 7:e51499, 2012.

[36]Pette, D., and G. Vrbova. Neural control of phenotypic expression in mammalian muscle fibers. *Muscle Nerve* 8:676–689, 1985.

[37]Powell, C. A., B. L. Smiley, J. Mills, and H. H. Vandenburgh. Mechanical stimulation improves tissue-engineered human skeletal muscle. *Am. J. Physiol. Cell Physiol.* 283:C1557–1565, 2002.

[38]Ramaswamy, K. S., M. L. Palmer, J. H. van der Meulen, A. Renoux, T. Y. Kostrominova, D. E. Michele, and J. A. Faulkner. Lateral transmission of force is impaired in skeletal muscles of dystrophic mice and very old rats. *J. Physiol.* 589:1195–1208, 2011.

[39]Rando, T. A. The dystrophin-glycoprotein complex, cellular signaling, and the regulation of cell survival in the muscular dystrophies. *Muscle Nerve* 24:1575–1594, 2001.

[40]Rhim, C., D. A. Lowell, M. C. Reedy, D. H. Slentz, S. J. Zhang, W. E. Kraus, and G. A. Truskey. Morphology and ultrastructure of differentiating three-dimensional mammalian skeletal muscle in a collagen gel. *Muscle Nerve* 36:71–80, 2007.

[41]Sanger, J. W., J. Wang, Y. Fan, J. White, and J. M. Sanger. Assembly and dynamics of myofibrils. *J. Biomed. Biotechnol.* 2010:858606, 2010.

[42]Schindelin, J., I. Arganda-Carreras, E. Frise, V. Kaynig, M. Longair, T. Pietzsch, S. Preibisch, C. Rueden, S. Saalfeld, B. Schmid, J. Y. Tinevez, D. J. White, V. Hartenstein, K. Eliceiri, P. Tomancak, and A. Cardona. Fiji: an open-source platform for biological-image analysis. *Nat. Methods* 9:676–682, 2012.

[43]Schultz, E. Fine structure of satellite cells in growing skeletal muscle. *Am. J. Anat.* 147:49–70, 1976.

[44]Sciandra, F., M. Bozzi, M. Bianchi, E. Pavoni, B. Giardina, and A. Brancaccio. Dystroglycan and muscular dystrophies related to the dystrophin-glycoprotein complex. *Ann. Ist. Super. Sanita.* 39:173–181, 2003.

[45]Sun, Y., R. Duffy, A. Lee, and A. W. Feinberg. Optimizing the structure and contractility of engineered skeletal muscle thin films. *Acta Biomater.* 9:7885–7894, 2013.

[46]Sun, Y., R. Duffy, A. Lee, and A. W. Feinberg. Optimizing the structure and contractility of engineered skeletal muscle thin films. *Acta Biomater.* 9:7885–7894, 2013.

[47]Szymanski, J. M., Q. Jallerat, and A. W. Feinberg. ECM protein nanofibers and nanostructures engineered using surface-initiated assembly. *J. Vis. Exp.* 86:e51176, 2014.

[48]Vandenburgh, H. H., P. Karlisch, and L. Farr. Maintenance of highly contractile tissue-cultured avian skeletal myotubes in collagen gel. *In Vitro Cell Dev. Biol.* 24:166–174, 1988.

[49]Vandenburgh, H., J. Shansky, F. Benesch-Lee, V. Barbata, J. Reid, L. Thorrez, R. Valentini, and G. Crawford. Drug-screening platform based on the contractility of tissue-engineered muscle. *Muscle Nerve* 37:438–447, 2008.

[50]Wang, P. Y., H. T. Yu, and W. B. Tsai. Modulation of alignment and differentiation of skeletal myoblasts by submicron ridges/grooves surface structure. *Biotechnol. Bioeng.* 106:285–294, 2010.

[51]Wilschut, K. J., H. P. Haagsman, and B. A. Roelen. Extracellular matrix components direct porcine muscle stem cell behavior. *Exp. Cell Res.* 316:341–352, 2010.

[52]Wolf, M. T., K. A. Daly, J. E. Reing, and S. F. Badylak. Biologic scaffold composed of skeletal muscle extracellular matrix. *Biomaterials* 33:2916–2925, 2012.

[53]Yaffe, D., and O. Saxel. Serial passaging and differentiation of myogenic cells isolated from dystrophic mouse muscle. *Nature* 270:725–727, 1977.

[54]Yamamoto, Y., A. Ito, M. Kato, Y. Kawabe, K. Shimizu, H. Fujita, E. Nagamori, and M. Kamihira. Preparation of artificial skeletal muscle tissues by a magnetic force-based tissue engineering technique. *J. Biosci. Bioeng.* 108:538–543, 2009.

[55]Zanotti, S., S. Saredi, A. Ruggieri, M. Fabbri, F. Blasevich, S. Romaggi, L. Morandi, and M. Mora. Altered extracellular matrix transcript expression and protein modulation in primary Duchenne muscular dystrophy myotubes. *Matrix Biol.* 26:615–624, 2007.

[56]Zatti, S., A. Zoso, E. Serena, C. Luni, E. Cimetta, and N. Elvassore. Micropatterning topology on soft substrates affects myoblast proliferation and differentiation. *Langmuir* 28:2718–2726, 2012.

[57]Zhao, Y., H. Zeng, J. Nam, and S. Agarwal. Fabrication of skeletal muscle constructs by topographic activation of cell alignment. *Biotechnol. Bioeng.* 102:624–631, 2009.

[58]Zou, K., M. De Lisio, M. A. Miller, D. Olatunbosun, E. Samuel, and M. D. Boppart. Laminin-111 improves skeletal muscle repair following eccentric exercise-induced damage. *Med. Sci. Sports Exerc.* 46:926–926, 2014.